

Influence of kink waves in solar magnetic flux tubes on spectral lines

S.R.O. Ploner and S.K. Solanki

Institut für Astronomie, ETH-Zentrum, CH-8092 Zürich, Switzerland

Received 18 November 1996 / Accepted 25 April 1997

Abstract. The kink-mode waves in solar magnetic flux tubes have been proposed as the carriers of significant amounts of energy into the upper atmosphere. Their observational signature, i.e. their influence on polarized spectral lines, is investigated theoretically using a simple MHD model and radiative transfer calculations. The results of a large model grid are presented. The wave is found to periodically shift, broaden, strengthen and change the asymmetry of circularly and linearly polarized profiles (Stokes V and Q , respectively). For most, but not all line parameters it exhibits its largest influence close to the limb. The time fluctuations of all quantities are in phase for Stokes Q and V , except for their amplitudes, which are in antiphase. The signal of the wave in time-averaged profiles depends on the wave frequency. Stokes Q and V exhibit opposite senses of the blue-red asymmetry and wavelength shift. This behaviour is found to be a result of the dependence on frequency of the phase relation between velocity and flux tube inclination. As the wave frequency approaches the cutoff frequency the phase relation changes and the time-averaged line asymmetry and shift decrease rapidly. High frequency kink waves are found to be an extremely efficient source of Stokes Q and V asymmetry, while maintaining a small line shift.

Key words: Sun: magnetic field – Sun: activity – Sun: flux tubes – Stokes radiative transfer – kink waves

1. Introduction

Waves in solar magnetic flux tubes (FTs) are of interest for a variety of reasons. For example, it is well established that they play an important role in channeling the energy from the convection zone to the chromosphere (e.g. Herbold et al., 1984, Choudhuri et al., 1993a, b) and may transport a significant fraction of the energy needed to heat the corona (e.g. Hollweg, 1991, Choudhuri et al., 1993b). A detailed knowledge of FT wave modes is therefore important for an understanding of heating mechanisms.

Send offprint requests to: S.R.O. Ploner

FT waves are predicted by theory to exist in different modes, with longitudinal (sausage) and transversal (kink and torsional) oscillations being the most important in thin flux tubes. In contrast to the well developed theory (e.g. Defouw, 1976; Roberts & Webb, 1978; Spruit, 1982; Thomas, 1985; Roberts, 1986, 1990; Ryutova, 1990; Ulmschneider et al., 1991; Ferriz Mas et al., 1989; Zhugzhda, 1996, see Roberts & Ulmschneider, 1996, for a review), FT waves are not always easy to observe. Excepted are sunspots, the largest flux tubes, which have been observed to harbour running penumbral waves (Zirin & Stein, 1972; Giovanelli, 1972), magneto-atmospheric modes (Lites, 1992) and probably Alfvénic surface modes (Ulrich, 1996). The difficulty of spatially resolving small FTs forming plages and the network (the FT radii of about 100 – 300 km lie below the spatial resolution limit of most observations) has hindered the direct detection of their wave modes. Nevertheless, various observers have reported oscillatory motions in small FTs, mainly longitudinal tube modes at a period of 5 minutes (e.g. Giovanelli et al., 1978; Deubner, 1991; Fleck & Deubner, 1991; cf. Roberts, 1983), although recently evidence for shorter period waves was also found (Volkmer et al., 1995). Note that polarization measurements may yield information on magnetic structures smaller than the spatial resolution limit.

There are only few studies that attempt to bridge the gap between theory and observations, i.e. which use theory to predict the detailed signature of various wave modes. Such predictions are required to find new techniques for observing the waves and improving estimates of the energy flux transported by them. Simulations of line profiles disturbed by longitudinal waves have been presented by Rammacher & Ulmschneider (1989) and Rammacher (1991) for Mg II k and Ca II K and by Solanki & Roberts (1992) for Stokes I and V profiles of photospheric lines. For other FT wave modes only Steiner et al. (1995, 1996) have presented and discussed line profiles formed in the presence of kinked flux slabs. Their 2-D MHD simulations incorporate considerable physical realism. In the present paper we consider the polarimetric signature of kink waves in thin FTs on the basis of a simpler and less realistic model than Steiner et al. (1995, 1996). On the other hand, our approach allows us to study a whole grid of wave and line parameters. This

paper may thus be considered to be an extension of the work of Solanki & Roberts (1992) on the longitudinal tube mode to the kink mode, as well as complementary to the approach taken by Steiner et al. (1995, 1996).

In the context of chromospheric and coronal heating kink waves are of greater interest than longitudinal tube waves: The kink mode has a much lower cut-off frequency, so that propagating kink waves are more likely to be excited by granular buffeting than longitudinal tube waves (Spruit, 1981). The importance of rapid foot points motion of FTs as efficient excitors of kink modes above their cut-off frequency has been pointed out by Choudhuri et al. (1993a). The tilts and shifts produced in isolated FTs by such buffeting are demonstrated dramatically by the 2-D simulations of Steiner et al. (1994). Another interesting aspect of kink waves is that they do not suffer from radiative damping, nor do they shock in the chromospheric layers. They may thus be interesting for coronal heating (Spruit, 1981; Hollweg, 1991). Kink modes may, nevertheless, also be important for chromospheric heating through their non-linear coupling with longitudinal modes (Ulmschneider et al., 1991). These shock and dissipate very efficiently in the chromospheric layers.

2. The model

2.1. Kink waves

We first consider a vertical thin FT in equilibrium and possessing a circular cross section. (A FT is thin when the pressure scale height is larger than the radius of the circular FT cross section.) The FT is assumed to have an untwisted magnetic field B . For a vertical thin FT horizontal force balance reduces to pressure equilibrium,

$$p_e = p_i + \frac{B^2}{8\pi}. \quad (1)$$

In Eq. (1) p_e and p_i are the external and internal gas pressure, respectively. If all displacements are small then the propagation of a kink mode oscillation of the above FT is described by (Spruit, 1981)

$$\frac{\partial^2}{\partial t^2} \zeta(z, t) = g \frac{\rho_i - \rho_e}{\rho_i + \rho_e} \frac{\partial}{\partial z} \zeta(z, t) + \frac{\rho_i}{\rho_i + \rho_e} v_A^2 \frac{\partial^2}{\partial z^2} \zeta(z, t). \quad (2)$$

Here $\zeta(z, t)$ is the horizontal displacement at the height z and time t , ρ_i the density inside the FT, ρ_e the density of the field-free external plasma, g the gravitational acceleration and $v_A^2 = B^2/4\pi\rho_i$ the Alfvén speed inside the FT. The first term on the right-hand-side describes the effects of gravitation and stratification by means of buoyancy; the second term includes the restoring forces of the magnetic field. To account for the back-reaction of the external plasma onto the FT, the orthogonal force acts on $\rho_e + \rho_i$ (the sum of the external and internal density) instead of on ρ_i alone, where ρ_e represents the increase of inertia for a potential flow around a circular cylinder.

Spruit solved Eq. (2) for isothermal atmospheres, for which the pressure scale height H and the Alfvén velocity v_A are

independent of height z and the internal and external atmospheres are governed by the same pressure scale height H so that $p_i/p_e = \rho_i/\rho_e$. Under this assumption the coefficients of Eq. (2) are height independent and the solution reads (Spruit, 1981)

$$\zeta(z, t) \propto \Re \left(\exp(i\omega t - ikz + \frac{z}{4H}) \right), \quad (3)$$

where \Re signifies the real part of a complex function. The corresponding dispersion relation is found to be

$$k^2 = \frac{1}{16H^2} \left(\frac{\omega^2}{\omega_c^2} - 1 \right), \quad \text{with } \omega_c^2 = \frac{g}{8H} \frac{1}{2\beta + 1}. \quad (4)$$

In Eq. (4) k is the wavenumber, ω_c the cut-off frequency and $\beta = 8\pi p_i/B^2$ the plasma beta. For propagating waves – the waves of greatest interest for the heating of the upper atmosphere – the wavenumber k must be real. This condition is only fulfilled for $\omega \geq \omega_c$.

2.2. The atmosphere in the presence of a kink wave

A kink wave excitation changes the direction of the magnetic field vector, the horizontal velocity inside the FT and the position of the FT, each as a function of height and time. We assume, for simplicity, that the oscillations do not affect the surroundings. Hence no velocities are induced outside the FT in our model. In order to isolate the signature of kink modes we also neglect other external motions, in particular granular flows. We emphasize, however, that Eq. (2) takes into account the back-reaction of the external material onto the FT. Note also that the polarized Stokes parameters, whose reaction to kink waves we are mainly interested in, are unaffected by velocities outside the FT, the exception being the blue-red asymmetry of the Stokes parameters (Solanki 1989). Equation (2) describes only isolated kink waves, i.e. it neglects the coupling between these and longitudinal waves. This assumption should be of little consequence for our results since we consider only the photosphere, whereas according to Ulmschneider et al., (1991) the coupling between the wave modes becomes significant only in the chromosphere.

We employ the solution for isothermal atmospheres (Eq. 3). With this approximation we avoid problems arising from partial reflections in higher layers. Effects due to departures from isothermality are expected to be minor over the height range of formation of the spectral lines. This approximation requires the wavelength to be small compared to the temperature scale height. A lower limit to the wavelength is provided by the tube radius due to the thin-tube approximation.

The displacement of the tube due to the wave is given by Eq. (3),

$$\zeta(z, t) = \zeta_0 \cos \varphi \exp \left(\frac{z + z_0}{4H} \right), \quad (5)$$

where $\varphi = \omega t - k(z + z_0)$, $z_0 = 270$ km and ζ_0 is the FT displacement's amplitude at $z = -270$ km, i.e. at $z + z_0 = 0$, the

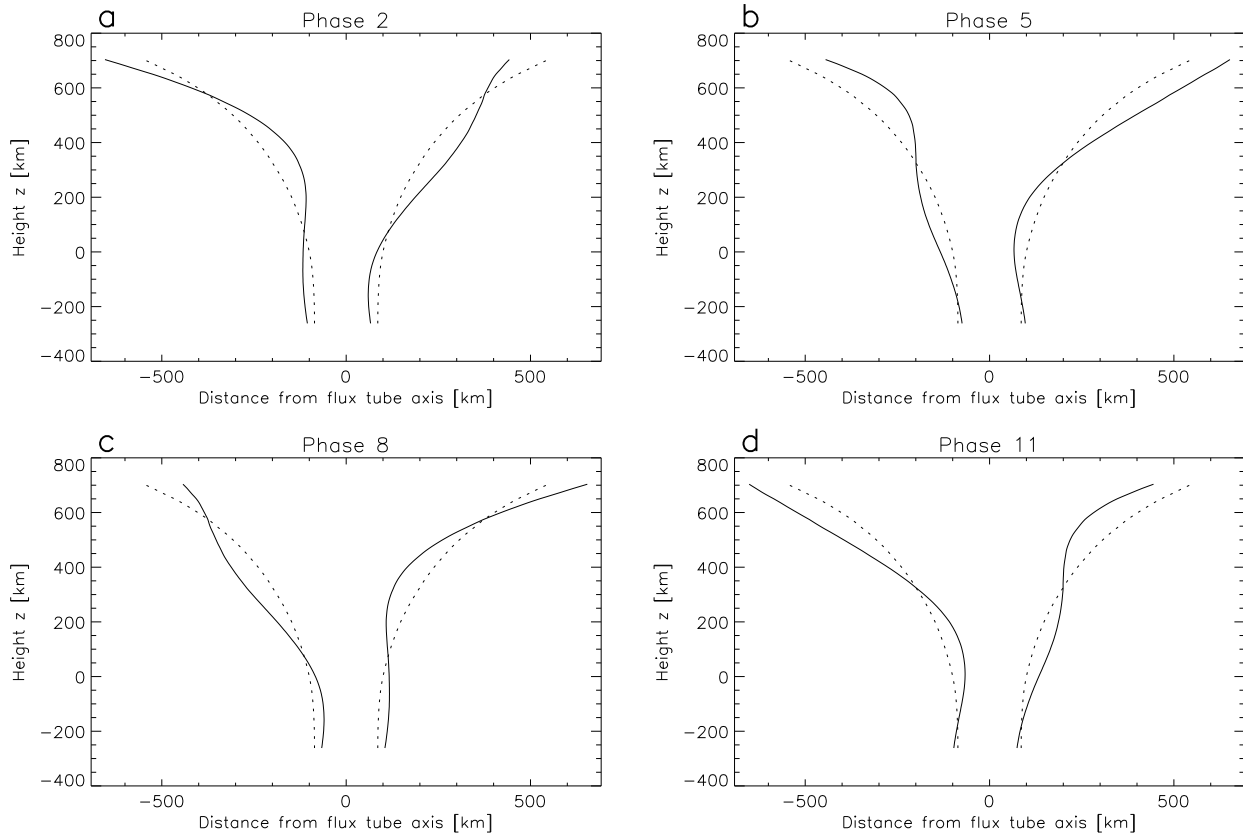


Fig. 1a–d. Vertical cut through a flux tube (FT) along a plane containing its axis and the direction of the displacement due to the kink wave. The dotted line represents the boundary of the unperturbed FT with $R = 100$ km at the lower end of the calculation domain, the solid line that of the FT distorted by a kink wave with $\omega = 0.04$ Hz ($\lambda \approx 1000$ km) and $v_0 = 0.9$ km s $^{-1}$, where ω is the wave frequency, λ the wavelength and v_0 the velocity amplitude at the lower end of the computational domain. The 4 frames correspond to phases at which the displacement vanishes or is largest at the estimated height ($z \approx 100$ km) of formation of Fe I 5250 Å. The height $z = 0$ corresponds to continuum optical depth unity in the quiet sun at 5000 Å ($\tau_{5000} = 1$)

lower end of the calculation domain. Taking the derivative with respect to time gives us the (horizontal) velocity,

$$v(z, t) = -v_0 \sin \varphi \exp\left(\frac{z+z_0}{4H}\right) \quad (6)$$

($v_0 = \omega \zeta_0$ denotes the velocity amplitude at $z = -270$ km), while the derivative with respect to z is a measure of the inclination of the FT axis relative to the vertical direction. The angle γ_0 between the magnetic field on the axis of the perturbed tube and the vertical is then given by

$$\tan \gamma_0(z, t) = \frac{\zeta_0}{4H} \left(\left(\frac{\omega^2}{\omega_c^2} - 1 \right)^{\frac{1}{2}} \sin \varphi + \cos \varphi \right) \times \exp\left(\frac{z+z_0}{4H}\right). \quad (7)$$

Here the wavenumber has been replaced using Eq. (4). In addition, γ also depends on the radial coordinate r , since the field is increasingly inclined at larger r (due to the expansion of the FT with height). Note that the cross section is not affected by

a linear kink wave. The additional inclination of the magnetic field away from the FT axis is

$$\tan \Delta\gamma(r, z) = \frac{r}{R(z)} \frac{\partial}{\partial z} (R(z)), \quad (8)$$

where $R(z)$ is the FT radius at z . The radius is calculated by means of flux conservation. Accordingly

$$\tan \gamma(r, z, t) = \tan \gamma_0(z, t) + \tan \Delta\gamma(r, z) \quad (9)$$

is the inclination of the magnetic field to the vertical at a distance r from the tube's central axis.

Fig. 1 shows a vertical cross section through the deformed FT at 4 phases for a given wave ($\omega = 0.04$ Hz, $v_0 = 0.9$ km s $^{-1}$). Fig. 2 exhibits ζ , γ , v and $\partial v/\partial z$ along the (deformed) axis of the FT at the same 4 phases. At the considered frequency the phase difference between v and γ is roughly 160° , while ζ and $\partial v/\partial z$ are approximately 90° out of phase. This agrees qualitatively with the more elaborate calculations of Ulmschneider et al. (1991). The phase difference between local maximum velocity and local maximum inclination depends on wave frequency.

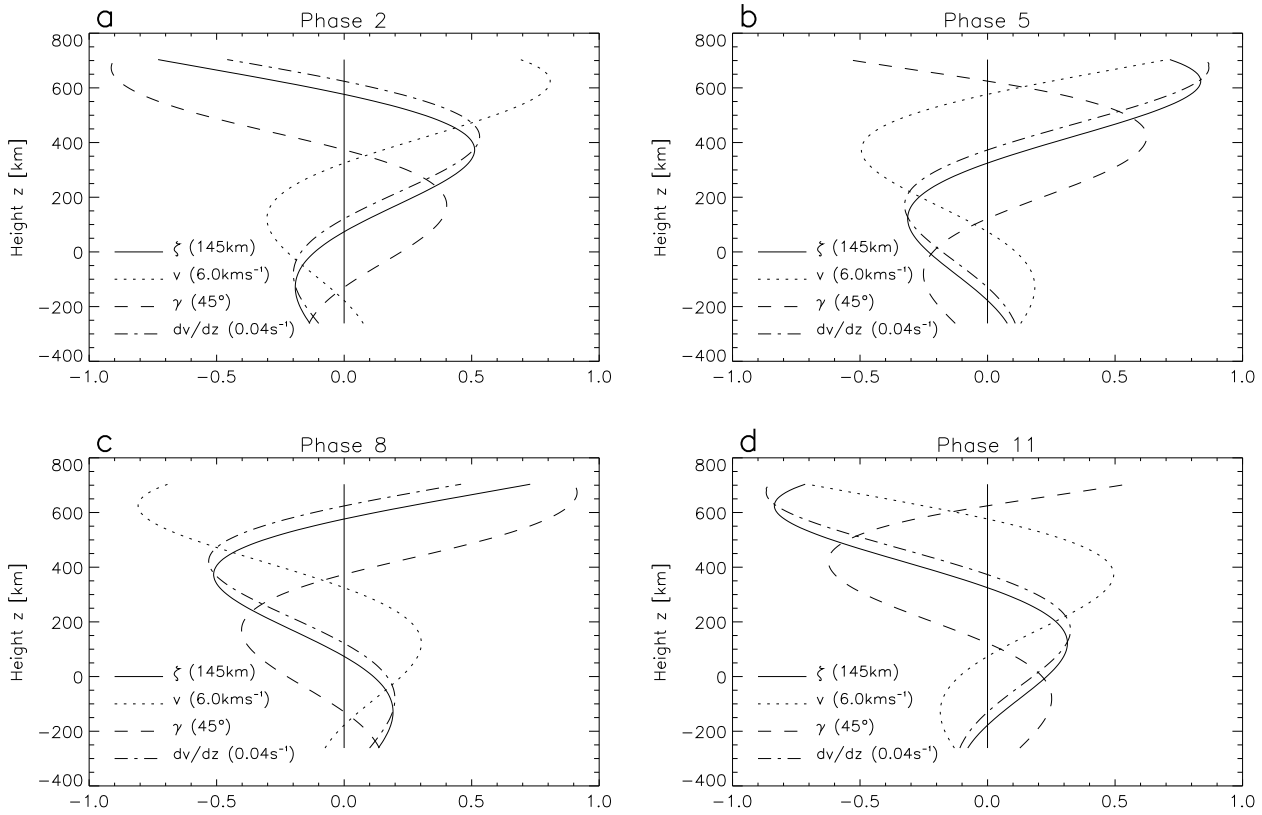


Fig. 2a–d. The horizontal displacement ζ , the horizontal velocity v , the inclination γ and the vertical gradient of the horizontal velocity $\partial v/\partial z$ at the FT axis vs. height z for the same wave as in Fig. 1. Each parameter is normalized by a factor that is indicated in the plots in brackets. The signs have been chosen such that positive magnitudes always indicate the direction away from the observer. Note that inside the flux tube the visible spectral lines we consider here are formed roughly within a range of about 150 km around a height of $z \approx 100$ km

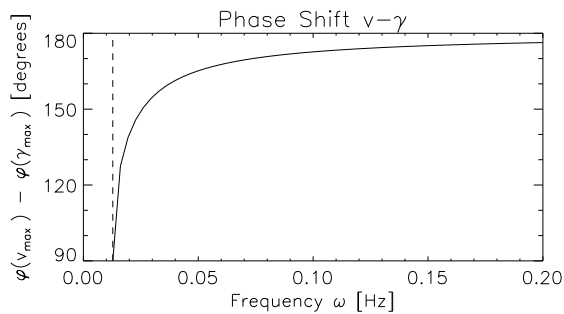


Fig. 3. The phase difference between local maximum velocity v_{\max} and local maximum inclination γ_{\max} of the FT axis vs. wave frequency. The vertical dashed line indicates the cut-off frequency, ω_c

Fig. 3 illustrates the strong change in the phase relation close to the cut-off frequency. For high wave frequencies ($\omega \gg \omega_c$) the sine term dominates in Eq. (7), giving rise to a phase difference of approximately 180° for an upward propagating wave. Near the cut-off frequency the cosine dominates in Eq. (7), so that velocity and inclination are nearly 90° out of phase even for $\omega > \omega_c$.

In order to obtain realistic line profiles we follow the same procedure as Solanki & Roberts (1992), i.e. we use empirically obtained atmospheres to describe the unperturbed FT, on which we superimpose the wave calculated in an isothermal atmosphere. The undoubted relevance of non-isothermal effects for line formation is thus taken into account, whereas such effects are assumed to play no role for the wave propagation. For the internal atmosphere we have used the plage FT model of Solanki & Brigljević (1992) with $B = 1500$ G imposed at $\log \tau(5000 \text{ \AA}) = 0$, in accordance with measurements of Rüedi et al. (1992). The external atmosphere is described by the empirical quiet-sun model of Maltby et al. (1986). The isothermal atmosphere for which the kink wave is calculated corresponds to the parameters of the plage FT model at a height of roughly $z = 50$ km. The pressure scale height is then $H = 128$ km, the plasma beta $\beta = 0.44$ and the cut-off frequency ω_c close to but smaller than 0.013 Hz (corresponding to a wave period of roughly 8 min).

2.3. Radiative transfer

We first intersect the FT with a grid of inclined mutually parallel rays (or lines-of-sight) lying in a plane containing the velocity vector and the vertical symmetry axis of the FT (compare with

Table 1. Atomic data of Fe I of the calculated spectral lines

λ [Å]	Transition	g_{eff}	χ_e [eV]	$\log gf$
5083.34	$a^3\text{F}_3 - z^3\text{F}_3^\circ$	1.25	0.96	-2.958
5250.21	$a^3\text{D}_0 - z^3\text{D}_1^\circ$	3.00	0.12	-4.933
15648.5	$e^7\text{D}_1 - 3d^64s5p^7\text{D}_1^\circ$	3.00	5.43	-0.70

Büntel et al., 1993). Only waves oscillating in the plane spanned by the FT axis and the line-of-sight are considered. Such waves are not easily visible at disc centre. Therefore, we simulate observations at different values of the heliocentric angle θ , the angle between the line-of-sight and the solar surface normal. We restrict ourselves to the rays in this central plane, since each wave also requires a full phase coverage, i.e. line profiles must be calculated at different phases in the wave, so that the computational load is significant. Test calculations suggest that this restriction should not affect our conclusions. The number of rays varied between 25 (for $\theta = 80^\circ$) and over 100 (for $\theta = 30^\circ$). It was dictated by the requirement that enough rays intersect the FT within the height range of line formation. Test calculations with more rays produced no significant change in the line profiles. Along each ray the data relevant to the radiative transfer are calculated as described by Bünte et al. (1993). Care is taken to keep the difference between the optical depth of neighbouring grid points constant. This increases the geometrical density of grid points at critical locations such as the FT boundaries. It is also ensured that there are sufficient grid points (typically at least 10) over the sometimes quite small height range over which a ray passes through the FT interior. For the present calculations we consider an array of FTs, a situation typical of active region plage. For simplicity we assume the whole array of FTs to oscillate in phase. Note that in this geometry a ray may enter a magnetic region more than once.

Stokes profiles are calculated in LTE with the code described by Solanki et al. (1992), which employs the Stokes Profile Synthesis Routine package (SPSR, Rees et al., 1989, Murphy & Rees, 1990, cf. Solanki, 1987 for details on other parts of the codes).

We concentrate here on Stokes V , the difference between right and left circular polarization, and Stokes Q parameters, the difference between linear polarization parallel and perpendicular to the limb in the polarization coordinates used here. In the selected geometry Stokes U signals are only due to magneto-optical effects and are not discussed further. Finally, Stokes I only exhibits a minute influence of the waves and is also not considered. In order to detect even subtle influences of kink waves on the Stokes profile we compare the perturbed profiles of each spectral line with profiles calculated in the unperturbed FT, which we call the reference line profiles.

Table 1 lists the three calculated spectral lines. Here λ is the solar wavelength of the transition, g_{eff} its effective Landé factor (note, however, that Fe I 5250 Å and Fe I 15648 Å are Zeeman triplets), and χ_e is the excitation potential of its lower level. The $\log gf$ values (oscillator strengths) are taken from

Thévenin (1989) and Solanki et al. (1992). Fe I 5250 Å is well known and often observed in magnetic features, Fe I 5083 Å is a stronger, more saturated spectral line, whose Stokes Q and V profiles should react more strongly to velocity gradients. It has been modeled by Bünte et al. (1993) in an only partially successful attempt to reproduce the centre-to-limb variation of its Stokes V asymmetry. Finally, Fe I 15648 Å is extremely Zeeman sensitive and is the most popular infrared line for magnetic measurements. It is formed considerably deeper in the atmosphere than the other lines. Each of the selected lines is expected to react differently to velocity gradients.

3. Results

We present results of a parameter study of kink waves and spectral lines formed in their presence. The influence of the following quantities on the Stokes profiles and their parameters is investigated:

1. The parameters determining the wave: These are the circular frequency ω lying in the interval between $\omega = 0.013$ Hz and 0.150 Hz, and the velocity at the bottom of the computational domain: $0.10 \text{ km s}^{-1} \leq v_0 \leq 1.30 \text{ km s}^{-1}$.
2. The angle between the line-of-sight and the vertical: $30^\circ \leq \theta \leq 80^\circ$.
3. The spectral line: Fe I 5083 Å, Fe I 5250 Å and Fe I 15648 Å.

We first focus on the time dependence of the Stokes Profiles (Sect. 3.1) and then define and discuss the line profile parameters at 12 time steps (named phases 0 to 11 in the following) within a wave period (Sect. 3.2). Later, in Sect. 3.3, the time averaged profiles and parameters are discussed for all three spectral lines.

3.1. Time evolution of Stokes profiles

Fig. 4 provides an overview of the time evolution of Stokes V (left hand panels) and Stokes Q (right hand panels) of all three spectral lines over one wave period. The response to the distorting wave exhibited by each spectral line is different. For example, Fe I 5083 Å shows little shift, but extreme variations in its σ -component amplitudes and in particular in its blue-red asymmetry. In contrast, the amplitude and asymmetry of Fe I 15648 Å varies only slightly. Instead, a considerable oscillatory line shift is present. Finally, Fe I 5250 Å exhibits an intermediate behaviour. Note that the flat cores of Fe I 5083 Å and Fe I 5250 Å are not due to excessive Zeeman splitting, but are the result of a combination of saturation, finite FT width and horizontally homogeneous external and internal atmosphere. (See Solanki et al. 1996 for details.) Fig. 4 also shows that some features of Stokes V and Q profiles oscillate in phase, others in anti-phase. For example, their wavelength shifts and blue-red asymmetries evolve in phase, but their amplitudes in anti-phase, i.e. the V profile is strongest when the Q profile is weakest and vice versa. In the following we study the quantitative response of the above and other line parameters to kink waves.

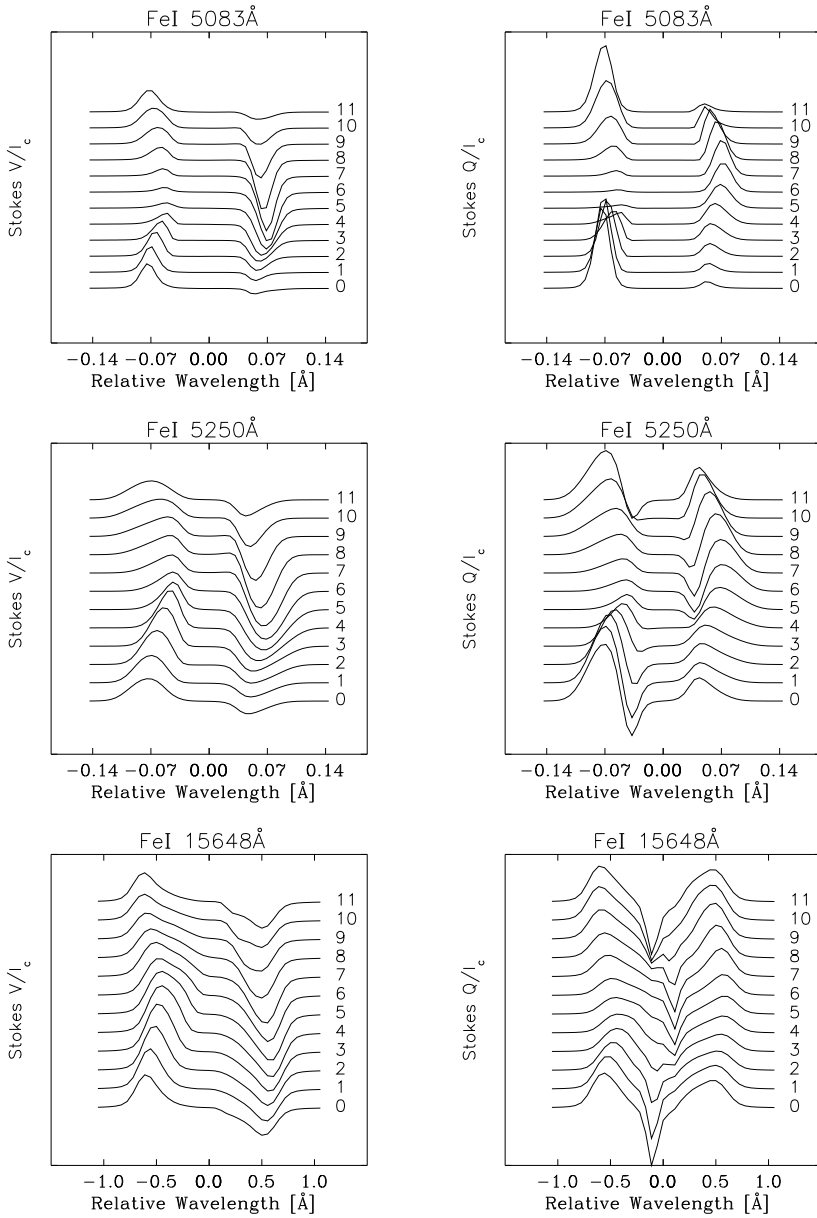


Fig. 4. Stackplots of the response of Stokes V (left-hand panels) and Stokes Q (right-hand panels) profiles of all three spectral lines to the same wave as in Fig. 1 are shown for 12 time steps covering one full wave period. All profiles are normalized to the continuum intensity I_c . The calculations correspond to a heliocentric angle $\theta = 60^\circ$. The profiles are off-set relative to each other for clarity. The time steps are marked at the right of each frame (time increases from 0 to 11)

3.2. Time evolution of line parameters

The evolution of a set of line parameters (defined below) with time over a full wave period is illustrated in Fig. 5a-j for the Fe I 5250 Å line. We first discuss the results for this line. As an example we have chosen an upward propagating wave with $v_0 = 0.9 \text{ km s}^{-1}$ and $\omega = 0.04 \text{ Hz}$, i.e. the same wave as in Figs. 1, 2 and 4. This frequency is sufficiently high that (according to Fig. 3) velocity and FT inclination are nearly in antiphase.

Definitions of the line profile parameters: The *line shift* $\Delta\lambda_\sigma = \frac{1}{2}(\lambda_r + \lambda_b)$, where $\lambda_{r,b}$ is the wavelength of the red, respectively blue σ -component peak (determined by placing a quadratic function through the 3 points closest to the peak) is plotted vs. time step or phase in Fig. 5a and b. We found this parameter to be superior to λ_V , the zero-crossing wavelength of Stokes V , and

λ_π , the wavelength of the π -component maximum of Stokes Q , as can easily be confirmed by considering the profiles of, e.g., Fe I 5083 Å in Fig. 4.

The most robust parameter describing the *line broadening* which we found is the difference between the centre-of-gravity wavelengths of blue and red σ -components:

$$\Delta\lambda_{cg} = \frac{1}{2} \left(\frac{\int_{\text{red}} \Delta\lambda |s(\lambda)| d\lambda}{\int_{\text{red}} |s(\lambda)| d\lambda} - \frac{\int_{\text{blue}} \Delta\lambda |s(\lambda)| d\lambda}{\int_{\text{blue}} |s(\lambda)| d\lambda} \right). \quad (10)$$

The function $s(\lambda)$ stands for Stokes Q or V and $\Delta\lambda$ for the unsigned wavelength relative to line-centre. After isolating the effects of the wave by removing the width of the reference line according to $\sqrt{\Delta\lambda_{cg}^2 - \Delta\lambda_{cg,ref}^2}$, the result is plotted in Fig. 5c and d. Since the magnetic field strength is not affected by the wave, we expect $\Delta\lambda_{cg}$ to be mainly influenced by velocity gra-

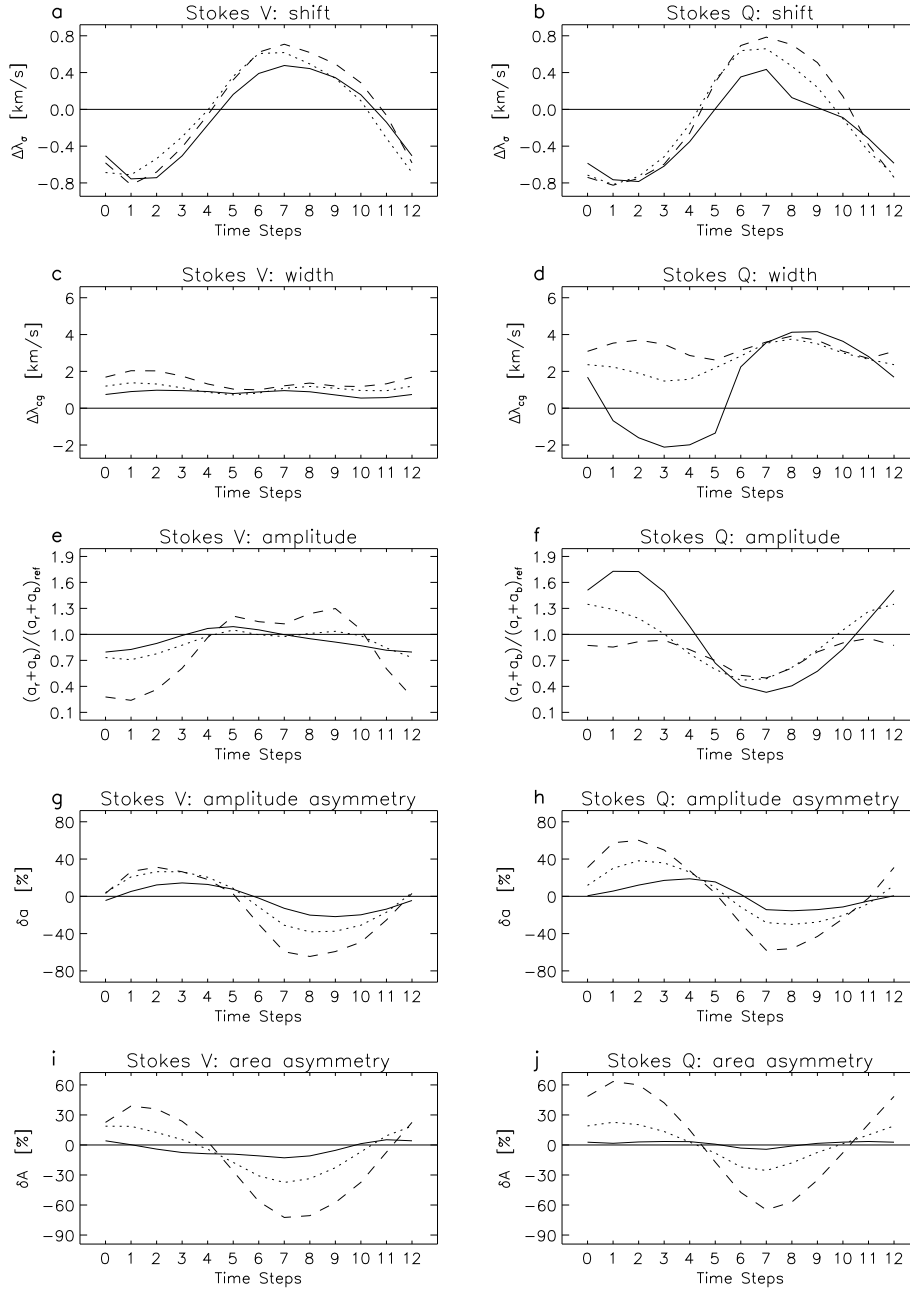


Fig. 5a–j. The evolution of the line profile parameters of Fe I 5250 Å over a single, full wave period is shown. The wave has frequency $\omega = 0.04$ Hz, wavelength $\lambda \approx 1000$ km and $v_0 = 0.9$ km s $^{-1}$, i.e. it is identical to the wave underlying Figs. 1, 2 and 4. Results are plotted for $\theta = 30^\circ$ (solid), $\theta = 50^\circ$ (dotted) and $\theta = 70^\circ$ (dashed). **a** to **j** present the response of various Stokes line parameters (left-hand panels Stokes *V* and right-hand panels Stokes *Q*). **a** and **b** show wavelength shifts, **c** and **d** line widths, **e** and **f** σ -component amplitudes, **g** and **h** blue-red relative amplitude asymmetry and **i** and **j** relative area asymmetry. The definitions of each of the plotted parameters is given in the text. Time steps are indicated on the horizontal axes. Step 12 represents the same phase as step 0

dients. Negative $\Delta\lambda_{cg}$ (we take the square root of the positive number and change the sign), which is occasionally seen in our calculations (see Stokes *Q* for $\theta = 30^\circ$), does not indicate that the line has been narrowed by the wave but rather signals a breakdown of the assumption of Gaussian profiles made above when removing the width of the reference profile. For example, the strength and width of the π -component, which is changed by the wave, has a significant effect on the $\Delta\lambda_{cg}$ of the *Q* profile.

The unsigned σ -component amplitudes are denoted by a_b and a_r , (where *b* and *r* indicate the blue and red σ -components, respectively). Fig. 5e and f show the variation of the total ampli-

tude normalized to the reference amplitude $(a_r + a_b)/(a_r + a_b)_{\text{ref}}$. The *relative amplitude asymmetry* δa , defined as

$$\delta a = \frac{a_b - a_r}{a_b + a_r}, \quad (11)$$

is plotted in Fig. 5g and h, while the time dependence of the *relative area asymmetry*,

$$\delta A = \frac{A_b - A_r}{A_b + A_r}, \quad (12)$$

is exhibited in Fig. 5i and j. Here, A_b and A_r are the unsigned areas of the blue and red σ -components, respectively.

Discussion of the line parameters: With the exception of $\Delta\lambda_{cg}$ all the line parameters plotted in Fig. 5 oscillate with the frequency of the wave. $\Delta\lambda_\sigma$, δa and δA also react approximately linearly to the sinusoidal wave, whereas the σ -amplitudes respond nonlinearly (the nonlinearity is more pronounced in Stokes V). In addition, most parameters possess maxima and minima around phases 1–2 and 7–8. Then the velocity around the estimated formation height of the σ -peaks of Fe I 5250 Å (≈ 100 km above the quiet-sun $\tau = 1$ level, as estimated from contribution function calculations) is largest and directed towards, respectively away from the observer (Fig. 2). Note, that the magnetic field is inclined towards the observer (at time step 8) and away from the observer (at step 2). This is reflected in the amplitudes of Stokes Q and V . Whereas all other line parameters of Stokes V oscillate in phase with those of Q , the amplitude of V is in antiphase with the amplitude of Q .

We now discuss the temporal behaviour of the line parameters in greater detail, in particular their dependence on wave frequency, heliocentric angle and spectral line. The dependence on velocity v_0 is discussed in Sect. 3.3.

Asymmetries and their production: In Fig. 5 the asymmetry parameters δa and δA of both Stokes Q and V reveal a nearly sinusoidal temporal behaviour. They all oscillate in phase and their oscillation amplitudes are roughly the same. In particular, the kink mode on its own does not enhance δa relative to δA . The asymmetries increase rapidly with increasing wave amplitude and even more rapidly with increasing θ and can approach 100%. The formation of such large asymmetries needs to be discussed in greater detail. Asymmetric Stokes profiles are efficiently produced by co-spatial gradients of line-of-sight velocity and magnetic field vector (Illing et al., 1975; Makita, 1986; Grossmann-Doerth et al., 1988; Sánchez Almeida & Lites, 1992; Solanki, 1993). In the present geometry we must differentiate between the abrupt field strength and velocity gradients at the FT boundary (which is crossed at least twice by each ray for sufficiently large θ values) and more gentle gradients in the field strength, inclination and velocity within the FT along each ray. For a kink wave the asymmetry produced at both the intersections of a slanted ray with the FT boundary has the same sign, as can easily be verified using the relation (e.g. Solanki, 1993)

$$\text{sign}(\delta A) = \text{sign}\left(-\frac{\partial v}{\partial \tau} \frac{\partial |B|}{\partial \tau}\right). \quad (13)$$

When viewed near the limb (large θ), therefore, gradients due to the kink waves at the flux tube boundaries are more efficient in producing δA in the present case than internal gradients or external granular flows (compare with Bünte et al., 1993). This explains the extremely large δA values produced by the wave (Fig. 5). The gradients at the FT boundaries also produce an amplitude asymmetry δa , which is generally of similar magnitude and sign as δA (e.g. Solanki, 1989).

Let us now discuss the influence of internal gradients on the production of asymmetries. Internal gradients are expected to have a stronger influence at higher wave frequencies, because

then, due to the shorter wavelength, the internal gradients are larger. Since the largest internal gradients of the velocity show a phase lag relative to maximum velocity we can test for the influence of internal gradients by checking whether the extrema in δa and/or δA occur at phases other than 2 and 8, at which the gradients across the FT boundary are largest. Fig. 5 shows that for small θ such a shift is present. It increases with wave frequency (not plotted) and is more pronounced in the amplitude asymmetry. Thus the influence of internal gradients relative to the jumps at the boundaries is largest at small θ , possibly due to the comparatively long path of a given ray within the FT. (But note that both the velocity gradients and the asymmetries get smaller for increasingly small θ).

The influence of the wave frequency: There are two effects caused by the wave frequency. Firstly, the frequency determines the phase lag between velocity v and magnetic field inclination γ (see Fig. 3). This phase lag controls the phase of maximum $a_b + a_r$ with respect to the phase of extreme $\Delta\lambda_\sigma$, δa and δA . For high frequencies, i.e. $\omega \gg \omega_c$, the maximum of $a_b + a_r$ occurs at roughly the same time as the extrema of $\Delta\lambda_\sigma$, δa and δA (cf. Fig. 5), whereas for frequencies close to the cut-off (not plotted) there is a significant temporal shift between the extrema of $a_b + a_r$ and those of $\Delta\lambda_\sigma$, δa and δA . At the lowest frequency we have considered, $\omega = 0.013$ Hz, we estimate this phase shift to be roughly a quarter of the wave period.

Secondly, as the wave frequency increases (and the wavelength accordingly decreases), the amplitudes of the oscillations exhibited by all line parameters decrease (for fixed wave velocity v_0). This is caused by the increasing ratio of the width of the line contribution (or response) function to the wavelength. In addition, with increasing wave frequency some parameters oscillate around an increasingly large, time independent offset. This is most obvious for the line shifts and the asymmetries.

Centre-to-limb variation: Whereas $\Delta\lambda_\sigma$ (line shift) shows little dependence on θ the other line parameters are significantly affected by it. For all parameters except the normalized amplitudes (Fig. 5e and f) Stokes Q and V show the same dependence on θ . The $(a_r + a_b)/(a_r + a_b)_{\text{ref}}$ oscillation amplitude of Q , however, is largest at small θ , while that of V is largest at large θ . We sketch out an explanation of this behaviour for an optically thin line (the results for an optically thick line are not expected to be too different). It is well known that Stokes $V \sim \cos \gamma$ and Stokes $Q \sim \sin^2 \gamma$, where γ is the angle between the line-of-sight and the magnetic vector. Now, γ oscillates as the FT sways back and forth over a wave period. The relative derivatives of Stokes Q and V according to γ are a measure of the change produced in the relative amplitudes of these profiles by changing γ : $\partial \ln V / \partial \gamma \sim \tan \gamma$ and $\partial \ln Q / \partial \gamma \sim \cot \gamma$. Hence we expect $\partial \ln(a_r + a_b) / \partial \gamma \sim \tan \gamma$ for Stokes V and $\sim \cot \gamma$ for Q . This difference in sensitivity to changes in γ between Stokes Q and V amplitudes agrees well with Fig. 5e and f.

FT inclination: The Stokes V and Q amplitudes are temporally in antiphase, as is clearly visible in Fig. 5e and f. This antiphase is expected due to their respective $\cos \gamma$ and $\sin^2 \gamma$ dependence. In other words Q is largest near the phase at which the FT is inclined away from the observer, while V is largest when it is inclined towards the observer. The ratio of the amplitude of Stokes Q to that of Stokes V , $(a_b(Q) + a_r(Q))/(a_b(V) + a_r(V))$, is plotted in Fig. 6. Note that the plotted curves have been divided by, i.e. normalized to, the Stokes Q to V ratio of the reference profile at the respective θ . The ratio follows the wave very clearly and obviously reflects the periodic swaying motion of the FT. The 3 lines exhibit a similar behaviour. Note, however, the (small) phase difference in inclination between the infrared and visible lines arising from the higher formation of the latter. At large θ this ratio exhibits extremely large fluctuations over a wave period. This has to do with the fact that the FT can become nearly perpendicular to the line-of-sight around phases 0–2, so that Stokes V (i.e. the denominator) becomes nearly zero at these phases.

Dependence on spectral line: There are considerable differences between the line profile parameters of the 3 spectral lines. For example, the line shift and line width of Fe I 5083 Å oscillates with a significantly smaller amplitude than the corresponding quantities of Fe I 5250 Å. The 5250 Å line itself shows smaller amplitudes of the $\Delta\lambda_\sigma$ and $\Delta\lambda_{cg}$ oscillations than the wave at this line's expected height of formation. This is in agreement with the expectation that the stronger line, Fe I 5083 Å, is formed over a larger range of height. For example, once the width of the contribution or velocity response function becomes of the order of the wavelength (the formation height range of $\Delta z \approx 150$ – 200 km has to be compared with $\lambda/4 \approx 250$ km for $\omega = 0.04$ Hz) the line shift increasingly fails to reflect the true amplitude of the wave. For the two visible lines, the amplitude (but not necessarily the time evolution) of the wave is more accurately reflected in $\Delta\lambda_{cg}$ than in $\Delta\lambda_\sigma$, in particular for larger wave frequency.

The amplitudes of the asymmetry oscillations are greater than in Fe I 5250 Å, due to the larger saturation in Fe I 5083 Å (Grossmann-Doerth et al., 1989; Solanki, 1989). In addition, Fe I 5083 Å reacts more sensitively to changes in wave frequency.

The response of Fe I 15648 Å differs substantially from that of the other two lines. The amplitude of the line shift corresponds closely to the wave amplitude around the level of line formation. The asymmetry produced by the wave is, in contrast, exceedingly small. This behaviour can be understood in terms of the relative weakness of the line and its large Zeeman splitting (Grossmann-Doerth et al., 1989).

3.3. Temporally averaged profiles

Consider now Stokes Q and V profiles averaged over a full wave period. On the one hand this corresponds to time averaged measurements, on the other hand to a snapshot of many

FTs caught at random phases, such as produced by observations with moderate spatial resolution. In Fig. 7 we plot Stokes V and Q profiles of Fe I 5250 Å averaged over a wave period. In the upper panels (Fig. 7a and b) we illustrate the influence of wave frequency, in the lower panels (Figs. 7c and d) the influence of the wave amplitude. Figs. 7a and b show asymmetric profiles at high frequencies and a transition to more symmetric profiles at frequencies close to the cut-off. (We emphasize, however, that waves with frequencies near the cut-off do not satisfy the approximation of an isothermal atmosphere and, therefore, should be used with caution.) Note that in Figs. 7a and b the frequencies are not equidistant. The velocity obviously affects the amplitude, asymmetry, broadening and shift of the lines (Figs. 7c and d). Note in particular the opposite sense of the asymmetry of Stokes V (red wing stronger than blue wing) and Q (blue stronger than red). This contrasts strikingly with the time-resolved profiles plotted in Fig. 4. Those Stokes V and Q profiles show the same sense of asymmetry at practically every phase (cf. Fig. 5). The temporally averaged V profiles also appear to be shifted towards the red, whereas the Q profiles are blue shifted, again in contrast to the time resolved profiles. The cause of this difference between the time resolved and time averaged profiles is discussed later in this section.

The same profile parameters as in Fig. 5, but now of temporally averaged profiles of different lines, are plotted vs. v_0 in Fig. 8a to j. This figure confirms that averaged over a wave period $\Delta\lambda_\sigma$, δa and δA of Stokes V are opposite in sign to the respective Q parameters. Note, however, that in general the net wavelength shift due to the wave is relatively small. On the other hand, the net Stokes Q and V asymmetry produced by even a modest amplitude wave is extremely large, unless the wave frequency lies very close to the cut-off.

In order to understand the opposite senses of δA , δa and $\Delta\lambda_\sigma$ of Stokes V relative to Q we must bear in mind that these parameters change sign over a wave period, with δA and δa being positive when the lines are blue shifted and negative for red shifted lines (Fig. 5). If we simply averaged these *line parameters* over a wave period then their values would be exceedingly small. If the *line profiles* are averaged the sign and magnitude of the net asymmetry and shift of the temporally averaged profiles is then determined mainly by the absolute amplitude $a_r + a_b$ of Stokes Q and V at different phases. The greater the amplitude of the Stokes profile at a certain phase the more it contributes to the average. The anti-phase of $a_r + a_b$ of Stokes Q and V (cf. Fig. 5) is responsible for the opposite sense of the line shift and asymmetry of Stokes V relative to that of Stokes Q . The basic reason for this behaviour is the 160° phase difference between wave velocity and FT inclination (Fig. 3) for this wave. This means that maximum inclination away from the observer (maximum Q) is cotemporal with maximum velocity away from the observer (maximum positive asymmetry) while minimum inclination (maximum V) is cotemporal with maximum velocity towards the observer (maximum negative asymmetry).

Next, let us compare the three spectral lines. As expected from the behaviour of the time resolved line parameters Fe I 5083 Å reacts most strongly to the kink mode, with the ex-

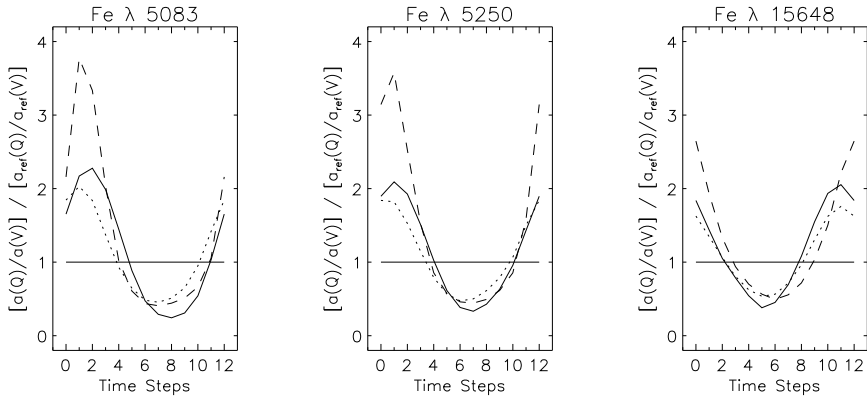


Fig. 6. The ratio of Stokes Q to V amplitude ($a_b(Q) + a_r(Q)$)/($a_b(V) + a_r(V)$) is plotted vs. time step for the lines Fe I 5083 Å (Fig. 6a), Fe I 5250 Å (Fig. 6b) and Fe I 15648 Å (Fig. 6c) for $\theta = 30^\circ$ (solid), 50° (dotted) and 70° (dashed). The wave parameters are $v_0 = 0.9 \text{ km s}^{-1}$ and $\omega = 0.04 \text{ Hz}$, i.e. the same as in Figs. 1, 2, 4 and 5. The amplitude ratio has been divided by the corresponding ratio of the reference profiles at the same θ

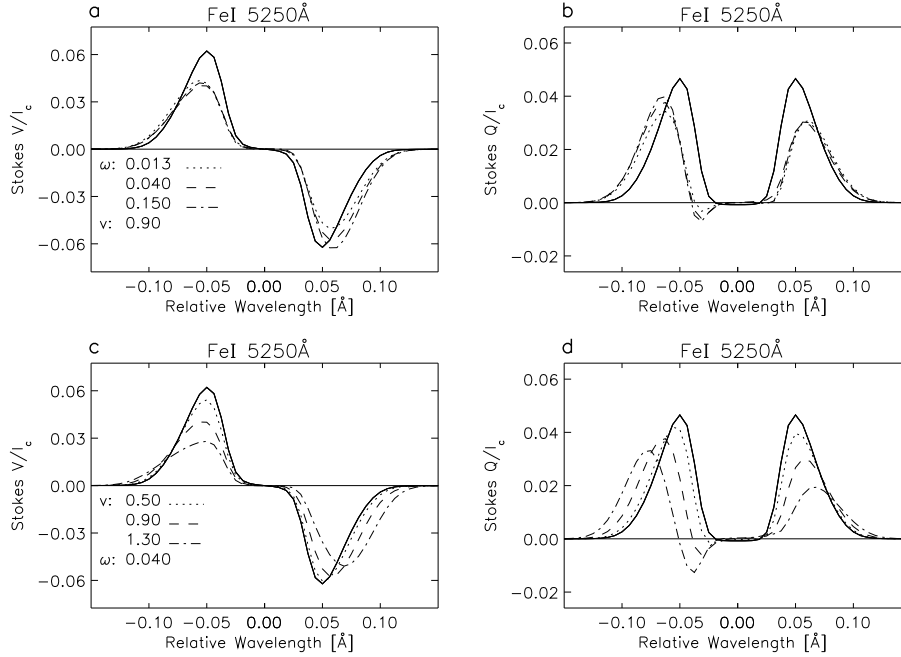


Fig. 7a–d. Temporally averaged Stokes V/I_c (a) and Q/I_c (b) profiles are plotted for waves with $v_0 = 0.9 \text{ km s}^{-1}$ and different wave frequencies indicated in a in Hz. The radiative transfer was carried out for a heliocentric angle of $\theta = 60^\circ$. The solid curves denote the reference profile, i.e. the Stokes profile calculated in the absence of a wave. c and d show the same for fixed $\omega = 0.04 \text{ Hz}$ and different values of v_0 indicated in c in km s^{-1}

ception of the net line shift, which is smallest for this line (it also showed the smallest time-resolved shift). Note, in particular, that the Stokes V asymmetry of Fe I 5083 Å is more negative than that of Fe I 5250 Å at every θ . This is particularly interesting since the observations away from disk centre suggest that such is actually the case on the sun (Pantellini et al., 1988; Bünte et al., 1993), whereas the simulations of Bünte et al. (1993) show that using a purely granular model it is difficult to obtain the correct relative asymmetries.

Finally, note the almost linear dependence of the time-averaged line broadening on the wave velocity. $\Delta\lambda_{cg}$ is expected to scale as $2v_0 \sin \theta$. The calculated $\Delta\lambda_{cg}$ usually lies somewhat above this estimate, partly we expect due to the difference between the line formation height and the lower end of the calculation domain, to which v_0 refers.

In Fig. 9 we plot the centre-to-limb variation of the line parameters of Fe I 5250 Å for waves with a fixed velocity amplitude v_0 but different frequencies. The centre-to-limb variation of Stokes V is relatively easy to predict: $\Delta\lambda_\sigma$, $\Delta\lambda_{cg}$, δa and δA all increase monotonically towards the limb, exactly as ex-

pected for a kink wave running on a vertical FT. The behaviour of Stokes Q is at first sight more enigmatic. Only $\Delta\lambda_{cg}$ steadily increases towards the limb, whereas $\Delta\lambda_\sigma$ decreases and δa and δA initially increase with increasing θ , before decreasing again.

In order to understand this behaviour recall that the time-averaged parameters plotted in Fig. 9 are large when (among other things) there is a large *difference* in the strength or σ -amplitude of the Stokes V , respectively Q profiles at different phases in the wave (Fig. 5e and f). This difference in strength is produced by the oscillation of γ . We must thus consider how Stokes Q and V react to changes in γ , which has been discussed in Sect. 3.2. The sensitivity of the Stokes V relative amplitude to γ is largest near the limb, while the Stokes Q relative amplitude become increasingly independent of γ near the limb. The decrease (at large θ) in the Stokes Q asymmetry is consequently due to this insensitivity (Fig. 5). The initial increase of $\delta a(Q)$ and $\delta A(Q)$ with θ reflects the increase of the line-of-sight velocity gradients.

The dependence on wave frequency produces no major surprises. As expected, the smallest frequency dependence is ex-

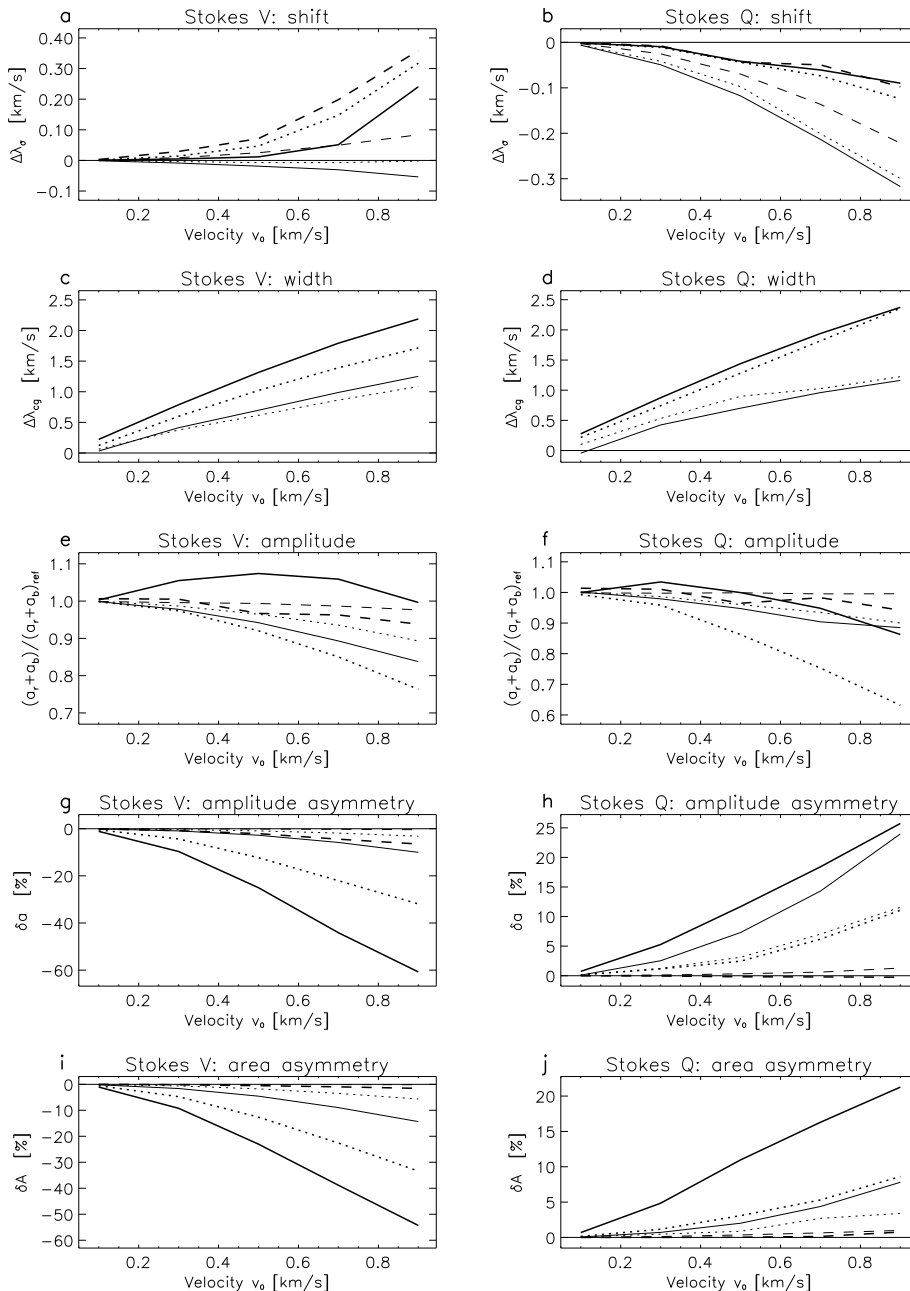


Fig. 8a–j. Parameters of temporally averaged Stokes V (left panels) and Q (right panels) profiles vs. v_0 for Fe I 5083 Å (solid), Fe I 5250 Å (dotted) and Fe I 15648 Å (dashed). The parameters and their order in the figure are the same as in Fig. 5. The plotted line parameters are affected by a wave with frequency $\omega = 0.04\text{Hz}$ ($\lambda \approx 1000\text{ km}$) “observed” at $\theta = 30^\circ$ (thin lines) and $\theta = 70^\circ$ (thick lines). Due to the large width of the reference profiles of Fe I 15648 Å (caused by Zeeman splitting), changes in $\Delta\lambda_{cg}$ due to the wave could not be well determined. The corresponding curves are not plotted in Fig. 8c and d

hibited by $\Delta\lambda_{cg}$ (which does not depend on the phase difference between velocity and inclination), whereas the asymmetries react most strongly to ω (particularly Stokes Q asymmetry). Also as expected, changes in ω values near ω_c have the largest influence on the line parameters. In addition, these low ω values produce the smallest line shift and asymmetries, due to the nearly 90° phase shift between velocity and FT inclination at these frequencies.

4. Conclusions

In the present study we have calculated linear, propagating kink-mode waves in thin flux tubes (FTs) and investigated the influ-

ence of the waves on the Stokes profiles and line parameters of three photospheric spectral lines. Most line parameters are strongly affected by kink waves. The profiles are considerably broadened and often exhibit large asymmetries, oscillations in amplitude and distorted σ -components.

We now summarize the most important features of the time-resolved line parameters, proceed with time-averaged profiles and conclude with a comparison to related research.

It is found that the line shift and the blue-red asymmetry of the σ -component amplitudes and areas of *temporally resolved* profiles quite clearly follow the wave (Fig. 5). These parameters oscillate in phase and have about the same magnitude for both Stokes Q and V . The Stokes Q and V amplitudes, how-

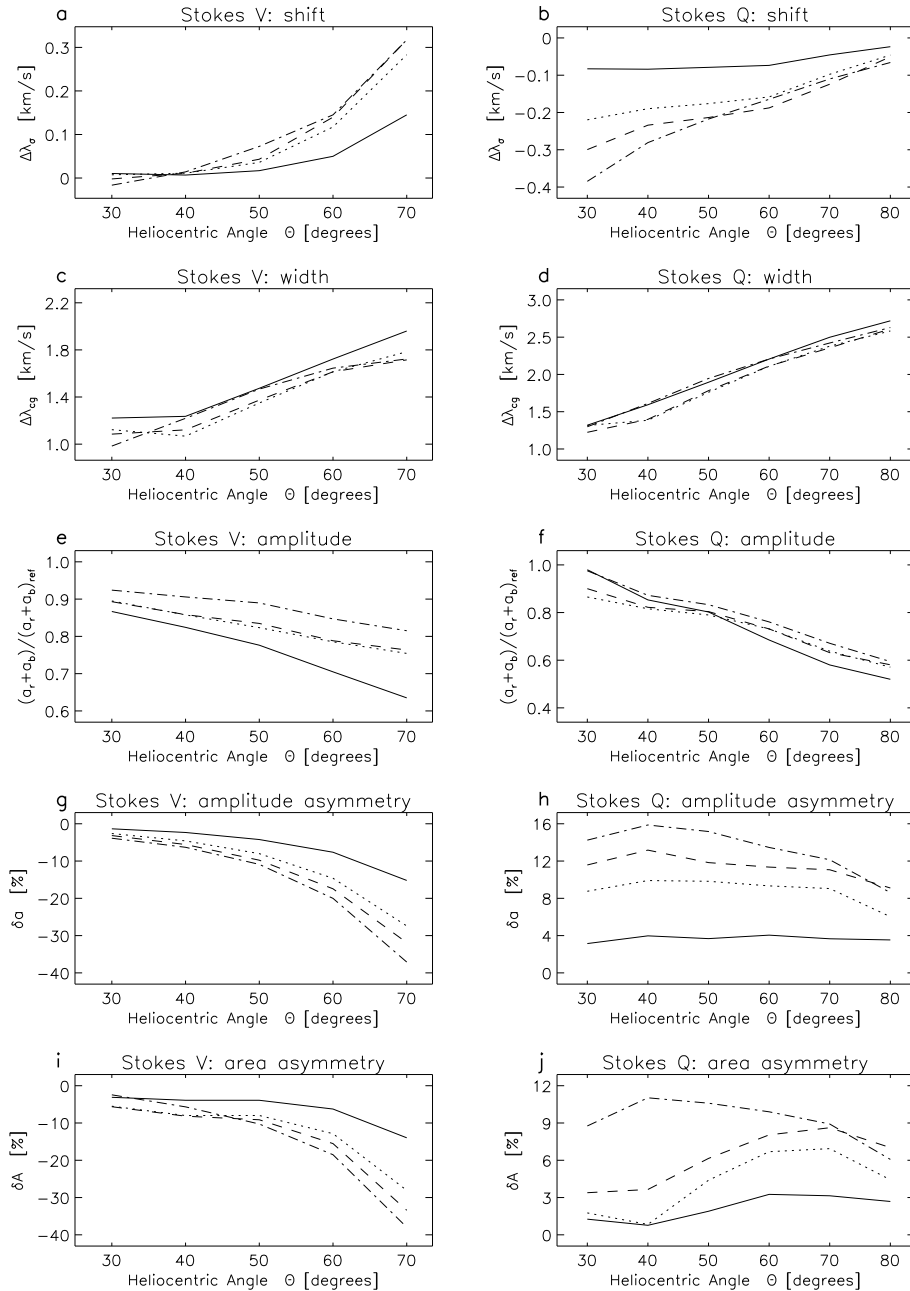


Fig. 9a–j. The same parameters of temporally averaged Stokes V and Q profiles of Fe15250 Å as in Figs. 5 and 8, but now plotted vs. θ . The parameters are calculated in the presence of waves with $v_0 = 0.9 \text{ km s}^{-1}$ and four different frequencies, $\omega = 0.013 \text{ Hz}$ (solid curves), $\omega = 0.02 \text{ Hz}$ (dotted), $\omega = 0.04 \text{ Hz}$ (dashed) and $\omega = 0.15 \text{ Hz}$ (dot-dashed). Note that the Stokes V parameters for $\theta = 80^\circ$ are not reliable since so close to the limb the wave causes the longitudinal component of the field and thus Stokes V to change sign periodically. Consequently, they have not been plotted

ever, oscillate in anti-phase. The response of the amplitudes is non-linear. For increasing wave frequency we observe increasing time-independent offsets around which all line parameters oscillate with increasingly smaller oscillation amplitudes. All the oscillation amplitudes are enhanced with increasing θ , except that of the Stokes Q amplitude, which exhibits the opposite centre-to-limb behaviour. A standard measure of the inclination of a FT, the ratio of the σ -components of Stokes Q to V , gives a particularly clear signature of the wave.

Kink waves also affect *time-averaged* line profiles (which also correspond to snapshots of many FTs oscillating at random phases). Surprisingly, an upward propagating wave produces a positive asymmetry in Stokes Q but a negative Stokes V asym-

metry. The Q and V line shifts also possess opposite signs. This seemingly contradictory behaviour is not seen in temporally resolved parameters, for which the two polarizations always respond in phase. The opposite asymmetries and shifts of Stokes Q and V are due to the antiphase of the oscillations of the Stokes Q and V amplitudes. The time-averaged asymmetries in Stokes V are generally larger than in Q .

The response of most line parameters of time averaged profiles is insignificant for waves with frequencies very close to the cut-off frequency – the line width, however, reacts equally strongly to waves of all frequencies. The reason for this dependence on frequency is the dependence of the phase relation between wave velocity and FT inclination on wave frequency.

Velocity and inclination are 180° out of phase for $\omega \gg \omega_c$, while for wave frequencies near the cut-off frequency the phase shift approaches 90° and remains there for standing waves. We conclude that standing waves or propagating kink modes with frequencies very near the cut-off hardly affect spatially unresolved measurements of asymmetries.

Consider now how the kink-mode signature differs from that of the tube mode investigated by Solanki & Roberts (1992). Most obviously the influence of the transverse kink mode increases towards the limb, while that of the longitudinal tube mode decreases. Another interesting difference is caused by the fact that the tube mode is compressible, whereas the kink mode is not. Due to the temperature variability accompanying compressibility the strength of a temperature-sensitive spectral line fluctuates over a wave period, while it remains essentially unchanged for kink-mode waves (excluding second-order effects). This causes the tube waves to have a much larger effect on the Stokes I profiles of temperature sensitive lines than kink waves.

Both wave modes produce an asymmetry in V and Q profiles. The sign of the blue-red asymmetry changes over a wave period. A net area and amplitude asymmetry can result even after averaging over a full wave period for both wave modes. In the case of the tube wave this is due to the fact that the velocity and temperature (or pressure) oscillate in phase for a propagating wave, while in the case of the kink wave it is the phase relation between the FT inclination and the velocity which is important. Note that in contrast to the tube wave the relevant phase shift of propagating kink waves changes dramatically with frequency near the cutoff.

Although both wave modes produce net blue-red asymmetric profiles, there are considerable differences between their signatures.

Firstly, the center-to-limb variation is expected to be very different. Secondly, the kink wave is more effective in producing asymmetric Stokes V and probably Q profiles. Thirdly, the ratio of amplitude to area asymmetry is much larger for the tube wave. Finally, whereas the two waves produce temporally averaged V with the same asymmetries for waves propagating in the same direction, say upwards, the sign of the Stokes Q asymmetry (for inclined lines of sight) is expected to differ. For the kink wave Q has the opposite asymmetry to V , while for the longitudinal wave we expect – from our understanding of the mechanisms producing the asymmetry – the Q profile to be asymmetric in the same sense as V . Note, however, that the kink-mode waves are not the only way of producing opposite asymmetry in V and Q (cf. Martínez Pillet et al. 1996).

One shortcoming of the present investigation is that we do not consider the combined effect of the wave and the surrounding granulation, or of different wave modes simultaneously present in the FT. Near the solar limb the granulation surrounding the FTs produces a Stokes V asymmetry of the same sign as an upward propagating kink wave, but the latter is more effective, particularly when we consider snapshots. Hence both mechanisms produce negative Stokes V asymmetry near the limb and thus enhance each other. They also produce approximately the same amplitude as area asymmetry, whereas

the observations show a significant negative area asymmetry but little amplitude asymmetry near the limb. Granulation and kink waves alone do not appear capable of removing this discrepancy.

How do the results of our simple model compare with the line profiles resulting from the sophisticated simulations of Steiner et al. (1994, 1995, 1996), whose simulations include the effects of non-stationary, supersonic convection, longitudinal shock waves and non-linear kink waves? Steiner et al. (1995) have also calculated Stokes profiles along lines of sight with $\theta = 60^\circ$. The main effect of the kink wave that they find is that it periodically produces large Stokes Q and V profiles (namely at the phases of maximum inclination of the FT, in agreement with our results). In addition, very close to the limb we also find Stokes V profiles with both σ -lobes having the same sign (cf. Steiner et al., 1995, Fig. 8, profile d). In our model such profiles are created when the FT is nearly perpendicular to the line-of-sight. Our calculations obviously miss, however, the rest of the dynamic phenomena distorting the line profiles in the Steiner et al. simulations.

The observations of Martínez Pillet et al. (1996) show the Q and V amplitude asymmetries to have the same sign for averages over many individual measured line profiles. This obviously cannot be accounted for by kink waves alone, since these produce opposite signs of δa . A mixture of kink waves and granulation, cannot, however, be ruled out, particularly since the temporally averaged Q asymmetry produced by the kink wave is significantly smaller than the V asymmetry (e.g. Fig. 8). Comparison of the relevant model calculation, which will be the subject of a future paper, with observations may be able to set limits on the energy flux transported into the upper atmosphere by kink-mode waves.

Acknowledgements. We thank M. Bunte for providing us with his code for intersecting a model FT with rays for radiative transfer. This work has been supported by grant No. 20-43048.95 of the Swiss National Science Foundation.

References

- Bunte M., Solanki S.K., Steiner O., 1993, A&A 268, 736
- Choudhuri A.R., Auffret H., Priest E.R., 1993a, Sol. Phys. 143, 49
- Choudhuri A.R., Dikpati M., Banerjee D., 1993b, ApJ 413, 811
- Defouw R.J., 1976, ApJ 209, 266
- Deubner F.-L., 1991, in Mechanisms of Chromospheric and Coronal Heating, P. Ulmschneider, E.R. Priest, R. Rosner (Eds.), Springer Verlag, Heidelberg, p. 6
- Ferriz Mas A., Schüssler M., Anton V., 1989, A&A 210, 425
- Fleck B., Deubner F.-L., 1991, in Mechanisms of Chromospheric and Coronal Heating, P. Ulmschneider, E.R. Priest, R. Rosner (Ed.), Springer Verlag, Heidelberg, p. 19
- Giovanelli R.G., 1972, Sol. Phys. 27, 71
- Giovanelli R.G., Livingston W.C., Harvey J.W., 1978, Sol. Phys. 59, 49
- Grossmann-Doerth U., Schüssler M., Solanki S.K., 1988, A&A 206, L37
- Grossmann-Doerth U., Schüssler M., Solanki S.K., 1989, A&A 221, 338

- Herbold G., Ulmschneider P., Spruit H.C., Rosner R., 1985, *A&A* 145, 157
- Hollweg J.V., 1991, in *Mechanisms of Chromospheric and Coronal Heating*, P. Ulmschneider, E. Priest, R. Rosner (Eds.), Springer-Verlag, Berlin, p. 423
- Illing R.M.E., Landman D.A., Mickey D.L., 1975, *A&A* 41, 183
- Lites B.W., 1992, in *Sunspots: Theory and Observations*, J.H. Thomas, N.O. Weiss (Eds.), Kluwer, Dordrecht, p. 261
- Makita M., 1986, *Sol. Phys.* 106, 269
- Maltby P., Avrett E.H., Carlsson M., Kjeldseth-Moe O., Kurucz R.L., Loeser R., 1986, *ApJ* 306, 284
- Martínez Pillet V., Lites B.W., Skumanich A., 1996, *ApJ* (in press)
- Murphy G.A., Rees D.E., 1990, *Operation of the Stokes Profile Synthesis Routine*, NCAR Technical Note, NCAR/TN-348+IA
- Pantellini F.G.E., Solanki S.K., Stenflo J.O., 1988, *A&A* 189, 263
- Rammacher W., 1991, in *Mechanisms of Chromospheric and Coronal Heating*, P. Ulmschneider, E.R. Priest, R. Rosner (Eds.), Springer Verlag, p. 414
- Rammacher W., Ulmschneider P., 1989, in *Solar and Stellar Granulation*, R. Rutten and G. Severino (Eds.), Reidel, Dordrecht, p. 589
- Rees D.E., Murphy G.A., Durrant C.J., 1989, *ApJ* 339, 1093
- Roberts B., 1983, *Sol. Phys.* 87, 77
- Roberts B., 1986, in *Small Scale Magnetic Flux Concentrations in the Solar Photosphere*, W. Deinzer, M. Knölker, H.H. Voigt (Eds.), Vandenhoeck & Ruprecht, Göttingen, p. 169
- Roberts B., 1990, in *Physics of Magnetic Flux Ropes*, C.T. Russell, E.R. Priest, L.C. Lee (Eds.), Geophysical Monograph 58, American Geophys. Union, Washington, DC, p. 113
- Roberts B., Ulmschneider P., 1996, in *Solar and Heliospheric Plasma Physics*, C.E. Alissandrakis, G. Simnett, L. Vlahos (Eds.), Lecture Notes in Physics, Springer-Verlag, Heidelberg, in press
- Roberts B., Webb A.R., 1978, *Sol. Phys.* 56, 5
- Rüedi I., Solanki S.K., Livingston W., Stenflo, J.O., 1992, *A&A* 263, 323
- Ryutova M.P., 1990, in *Solar Photosphere: Structure, Convection and Magnetic Fields*, J.O. Stenflo (Ed.), Kluwer, Dordrecht, IAU Symp. 138, 229
- Sánchez Almeida J., Lites B.W., 1992, *ApJ* 398, 359
- Solanki S.K., 1987, Ph.D. Thesis No. 8309, ETH, Zürich
- Solanki S.K., 1989, *A&A* 224, 225
- Solanki S.K., 1993, *Space Sci. Rev.* 63, 1
- Solanki S.K., 1996, in *Solar and Heliospheric Plasma Physics*, C.E. Alissandrakis, G. Simnett, L. Vlahos (Eds.), Lecture Notes in Physics, Springer-Verlag, Heidelberg, in press
- Solanki S.K., Brigljević V., 1992, *A&A* 262, L29
- Solanki S.K., Roberts B., 1992, *MNRAS* 256, 13
- Solanki S.K., Rüedi I., Livingston W., 1992, *A&A* 263, 312
- Solanki S.K., Steiner O., Bünte M., Murphy G., 1996, *A&A* submitted
- Spruit H.C., 1981, *A&A* 98, 155
- Spruit H.C., 1982, *Sol. Phys.* 75, 3
- Steiner O., Knölker M., Schüssler M., 1994, in *Solar Surface Magnetism*, R.J. Rutten and C.J. Schrijver (Eds.), p. 441
- Steiner O., Grossmann-Doerth U., Knölker M., Schüssler M., 1995 *Rev. Modern Astron.*, **8**, p. 81
- Steiner O., Grossmann-Doerth U., Schüssler M., Knölker M., 1996, *Sol. Phys.* 164, 223
- Thévenin F., 1989, *A&AS* 77, 137
- Thomas J.H., 1985, in *Theoretical Problems in High Resolution Solar Physics*, H.U. Schmidt (Ed.), Max Planck Inst. f. Astrophys., Munich, p. 126
- Ulmschneider P., Zähringer K., Musielak Z.E., 1991, *A&A* 241, 625
- Ulrich R.K., 1996, *ApJ* (in press)
- Volkmer R., Kneer F., Bendlin C., 1995, *A&A* 304, L1
- Zirin H., Stein A., 1972, *ApJ* 178, L85
- Zhugzhda Y. D., 1996, *Physics of Plasmas* **3**, 10